Int. J. Electrochem. Sci., 12 **(2017)** 5854 – 5866, doi: 10.20964/2017.07.83

International Journal of ELECTROCHEMICAL SCIENCE
www.electrochemsci.org

Effects of $Mo_{0.46}Fe_{0.54}$ Alloy on Microstructure and Electrochemical Hydrogen Storage Performances of $La_{0.75}Ce_{0.25}Ni_{4.2}Mn_{0.9-x}Cu_{0.3}(Mo_{0.46}Fe_{0.54})_x$ (x = 0-0.20) Alloys

Jianliang Cao[1], *Huanjian Xie*[1], *Zhihui Wen*[1,*], *Guohua Cao*[2], *Liqiang Ji*[3], *Yanping Fan*[1,*] *Baozhong Liu*[1]

[1] School of Chemistry and Chemical Engineering, Henan Polytechnic University, Jiaozuo 454000, China
[2] School of Physics & Electronic Information Engineering, Henan Polytechnic University, Jiaozuo 454000, China
[3] Inner Mongolia Rare Earth Ovonic Metal Hydride Co. Ltd., Baotou 014030, China
[*]E-mail: hpuforrest@hpu.edu.cn (Z. Wen); fanyanping@hpu.edu.cn (Y. Fan)

Received: 8 January 2017 / *Accepted:* 11 May 2017 / *Published:* 12 June 2017

The ratio of performance to price of $La_{0.7}Ce_{0.3}Ni_{4.2}Mn_{0.9}Cu_{0.3}$ hydrogen storage alloy was further optimized by substituting Mn with commercial $Mo_{0.46}Fe_{0.54}$ alloy, rather than pure Mo and Fe. Microstructures and electrochemical hydrogen storage properties of $La_{0.7}Ce_{0.3}Ni_{4.2}Mn_{0.9-x}Cu_{0.3}(Mo_{0.46}Fe_{0.54})_x$($x$ = 0-0.20) alloys are investigated. X-ray diffraction and backscattered electron results indicate that the pristine alloy is $LaNi_5$ phase with a hexagonal $CaCu_5$-type structure, while the alloys containing $Mo_{0.46}Fe_{0.54}$ consist of $LaNi_5$ matrix phase and a trace of Mo segregate phase. The lattice parameter a, c, c/a and V of $LaNi_5$ phase decrease after the addition of $Mo_{0.46}Fe_{0.54}$ alloy. As x increase from 0 to 0.20, maximum discharge capacity of alloy electrodes monotonically decreases from 332.5 (x = 0) to 310.2 (x = 0.20) mAh g^{-1}. The high-rate dischargeability the alloy electrodes at the discharge current density of 1200 mA g^{-1} first increases from 61.6% (x = 0) to 73.6% (x = 0.10), while further increasing the value of x jeopardizes HRD_{1200}. This is consistent with the variation tendency of hydrogen diffusion coefficient, which indicated that the electrochemical kinetic property is dominated by hydrogen atoms diffusion process in the bulk of alloy. The cycling capacity retention rate at the 100^{th} charge/discharge cycle is decrease monotonously from 79.3 % (x = 0) to 62.6 % (x = 0.20) with increasing the content of $Mo_{0.46}Fe_{0.54}$ alloy, which should be ascribed to the deterioration of corrosion resistance of alloy electrode in the charging/discharging cycle.

Keywords: Hydrogen storage alloy; Electrochemical properties; Kinetics; Microstructure; MoFe alloy

1. INTRODUCTION

In recent years, hydrogen-storage material has been widely used as electrode materials in the nickel-metal hydride battery (Ni/MH). AB_5-type hydrogen storage alloys, one of the most typical material, has been successfully applied to Ni/MH battery for portable electronic products, electric tools, electronic vehicles and power equipment owing to their high reversible hydrogen storage capacity, good activation performance and favorable high-rate property. However, despite the fact that AB_5-type hydrogen storage alloys can match many criteria for the negative electrodes material in Ni/MH batteries, the high cost of alloy clearly limits its applications to large-scale problems so that it cannot meet the increasing demands of an emerging market [1-3]. Worst of all, Ni/MH battery is encountering serious competition from high energy density Li-ion battery and lower price Ni-Cd battery. Therefore, reducing the cost play a crucial role for the development of AB_5-type hydrogen storage alloy.

To date, the Co-free high-Mn alloys were developed and commercially produced [4] because of manganese element is an indispensable element for the electrochemical property of AB_5-type hydrogen storage alloys [5,6], especially for maintaining cycle stability [7] and high-rate dischargeability (HRD) [8,9]. However, the high content of manganese element will raise the cost price of raw material and the electrochemical performances, especially high-rate dischargeability are not yet satisfying. Therefore, further reduce the cost and improve the overall electrochemical properties of Co-free high-Mn AB_5-type alloys is quite necessary and urgent. Out of the many methods for reducing the cost methods in existence, element substitution is one of the most effective methods which is use a different cheap commercial alloy or cost-effective substitute element to replace all or partial pure element. For example, Mi et al. [10] and Yan et al. [11] utilized commercial ferrovanadium alloy as a vanadium source to substitute the pure vanadium for reducing the cost of Ti-V based BCC alloy. Zhang et al. [12-14] reported that the cost-effective AlMo alloy to replace pure nickel element in La-Mg-Ni hydrogen storage alloy. The results showed that AlMo alloy can not only decrease the price of alloy but also increase the electrochemical properties of La-Mg-Ni alloy with increasing the content of AlMo to some extent. In our previous works [15,16], the commercial BFe and VFe alloys, rather than pure B, V or Fe, was used to substitute the Co, which substantially reduces the cost of the alloys and the electrochemical hydrogen storage performance was achieved.

Among the substitute elements, molybdenum element plays an important role in many aspects because of its superior characteristic as hydrogen-absorption. For example, Díaz et al. [17] reported that Mo has a positive effect for $LaNi_{3.6}Co_{0.7}Mn_{.4-x}Al_{0.3}Mo_x$ alloys. After the replacement of Mn by Mo, the alloy (2% w/w) presents an excellent discharge capacity and high-rate dischargeability and a lower charge-transfer resistance. Ye et al. [18,19] has also demonstrated that Mo-substitution can increase the room temperature high-rate dischargeability due to the increase in the exchange-current density without the degradation of the discharge capacity of alloy at low current density. Furthermore, Yeh et al. [20] and Hsu et al. [21] researched that the replacement of Ni and Co by Mo in Lm(Ni, Mn, Co, $Al)_{5-x}Mo_x$ and $Lm(Ni_{1-x}Mo_x)_5$ alloys and found that the hydrogen storage capacities and equilibrium plateau pressure of alloys at 313 K were improved. Obviously, molybdenum element is beneficial to electrochemical properties of AB_5-type hydrogen storage alloy, especially for the discharge capacity and high-rate dischargeability.

A commercial available $Mo_{0.46}Fe_{0.54}$ alloy is selected to substitute pure Mn element in Co-free high-Mn hydrogen storage alloy because of its cost-competitive and lower melt point compared with pure Mo can increase the performance/price ratio and contribute to the homogeneity of the alloys. More importantly, iron element is also beneficial for improving electrochemical properties of AB_5-type alloys [22,23], which due to its atomic radius, number of electrons, and electro-negativity being similar to those of Ni and Co. For example, it was reported that Fe introduction in AB_5 alloy can remarkably improve cycling stability due to the improvement in the anti-pulverization of the alloy electrode [24].

Here in, $La_{0.7}Ce_{0.3}Ni_{4.2}Mn_{0.9-x}Cu_{0.3}(Mo_{0.46}Fe_{0.54})_x$($x$ = 0-0.20) alloy is prepared by a vacuum arc melting furnace. For the sake of clarifying the role of new incorporation of $Mo_{0.46}Fe_{0.54}$, the microstructures and electrochemical hydrogen storage properties of the alloys are investigated in detail.

2. EXPERIMENT DETAIL

2.1 Alloys preparation

$La_{0.7}Ce_{0.3}Ni_{4.2}Mn_{0.9-x}Cu_{0.3}(Mo_{0.46}Fe_{0.54})_x$($x$ = 0-0.20) alloys were synthesized by arc melting in a water-cooled copper hearth under Ar atmosphere. The pure metals (La, Ce, Ni, Mn Cu: 99.9% in purity) and Mo-Fe alloy (46 at.% Mo and the other were Fe and trace impurities) were used as raw materials. A slight excess of Mn was used due to the oxidized loss during the process. The cast ingots were annealed at 1223 K for 6 h under Ar atmosphere with 0.8 MPa in the heat-treating furnace.

2.2 Microstructure characterization

The alloys of <400 mesh size obtained by hand grind in glove box (H2O,O2 less than 1 ppm) were used for X-ray diffraction (XRD) measurements, which were performed on an X'pert PROMPD XRD with Cu Kα radiation. The range of 2θ was 20° ~ 90° and the scanning rate was 0.02° min-1. Back scattered electron (BSE) images were measured by using HITACHI-4800 scanning electron microscope with an energy dispersive X-ray spectrometer (EDS).

2.3 PCT measurements

A volumetric method on a Sieverts-type apparatus was used to study the PCT curves of the alloys. Before the PCT curves measurement, the alloys were activated by the 5 hydring/dehydriding cycles at 303 K. During activated process, the initial hydriding pressure is ~2 MPa and the dehydriding one is ~0.001 MPa. The PCT curves were measured at 303K with the delay time of 180 s and the maximum pressure of 2 MPa.

2.4 Electrochemical measurements

The preparation methods and the measuring conditions of alloy electrodes was similar to the literature [15,16]. Electrochemical impedance spectrums (EIS), Tafel curves and potential-step

discharging were performed on an electrochemical workstation (PARSTAT 2273) at 298 K. The EIS were tested in the frequency range of 100 kHz to 10 mHz at 50% depth of discharge. The Tafel curves were measured at 100% depth of discharge with the scanning range of -250 mV (vs. Open circuit potential) to 250 mV (vs. Open circuit potential), and the scanning rate was 5 mV s-1. During the potential-step discharging process, the electrodes is fully charged state, and the potential steps were +500 mV (vs. Open circuit potential).

3. RESULTS AND DISCUSSION

3.1 Crystal structure

Fig. 1 shows the X-ray diffraction patterns of $La_{0.7}Ce_{0.3}Ni_{4.2}Mn_{0.9-x}Cu_{0.3}(Mo_{0.46}Fe_{0.54})$($x$= 0-0.20) alloys and the lattice parameters and unit cell volumes of alloy phase are listed in Table 1. It can be seen that all the alloys have a single the $LaNi_5$ phase with the $CaCu_5$-type hexagonal structures. It is noted that the a, c, c/a and V of the alloys decrease after the addition of $Mo_{0.46}Fe_{0.54}$ alloy. Fig. 2 shows the BSE micrographs of the $La_{0.7}Ce_{0.3}Ni_{4.2}Mn_{0.75}Cu_{0.3}(Mo_{0.46}Fe_{0.54})_{0.15}$ alloy. It can be seen that the BSE micrographs of $La_{0.7}Ce_{0.3}Ni_{4.2}Mn_{0.75}Cu_{0.3}(Mo_{0.46}Fe_{0.54})_{0.15}$ alloy consists of a mass of black grey area with sporadically distributed small quantity of white spots. Fig. 2 b-c shows EDS result of the two different area in $La_{0.7}Ce_{0.3}Ni_{4.2}Mn_{0.75}Cu_{0.3}(Mo_{0.46}Fe_{0.54})_{0.15}$ alloy. Combining the results of XRD, BSE micrographs and EDS analysis can conclude that the black grey area is $LaNi_5$ matrix phase and the sporadic white spot is Mo segregate phase. The same result was found by Young [25].

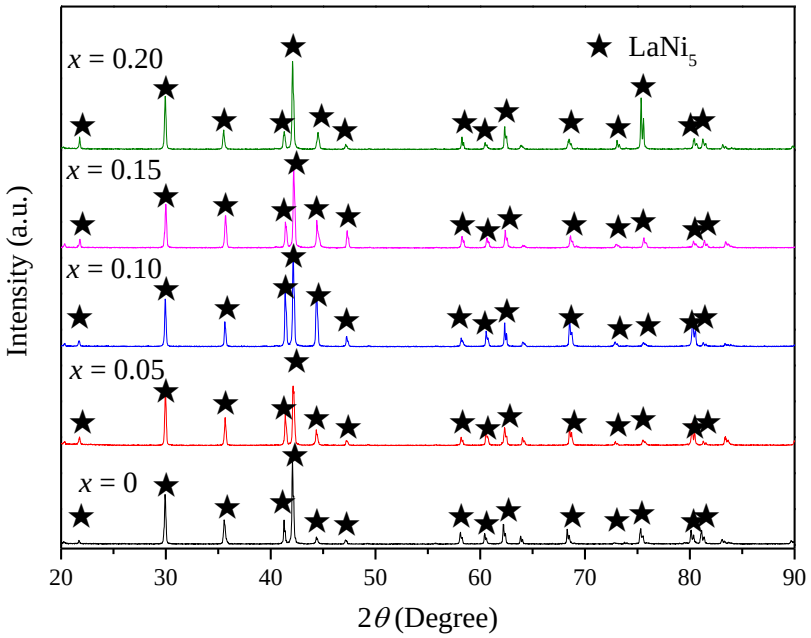

Figure 1. XRD patterns of $La_{0.7}Ce_{0.3}Ni_{4.2}Mn_{0.9-x}Cu_{0.3}(Mo_{0.54}Fe_{0.46})_x$ alloys

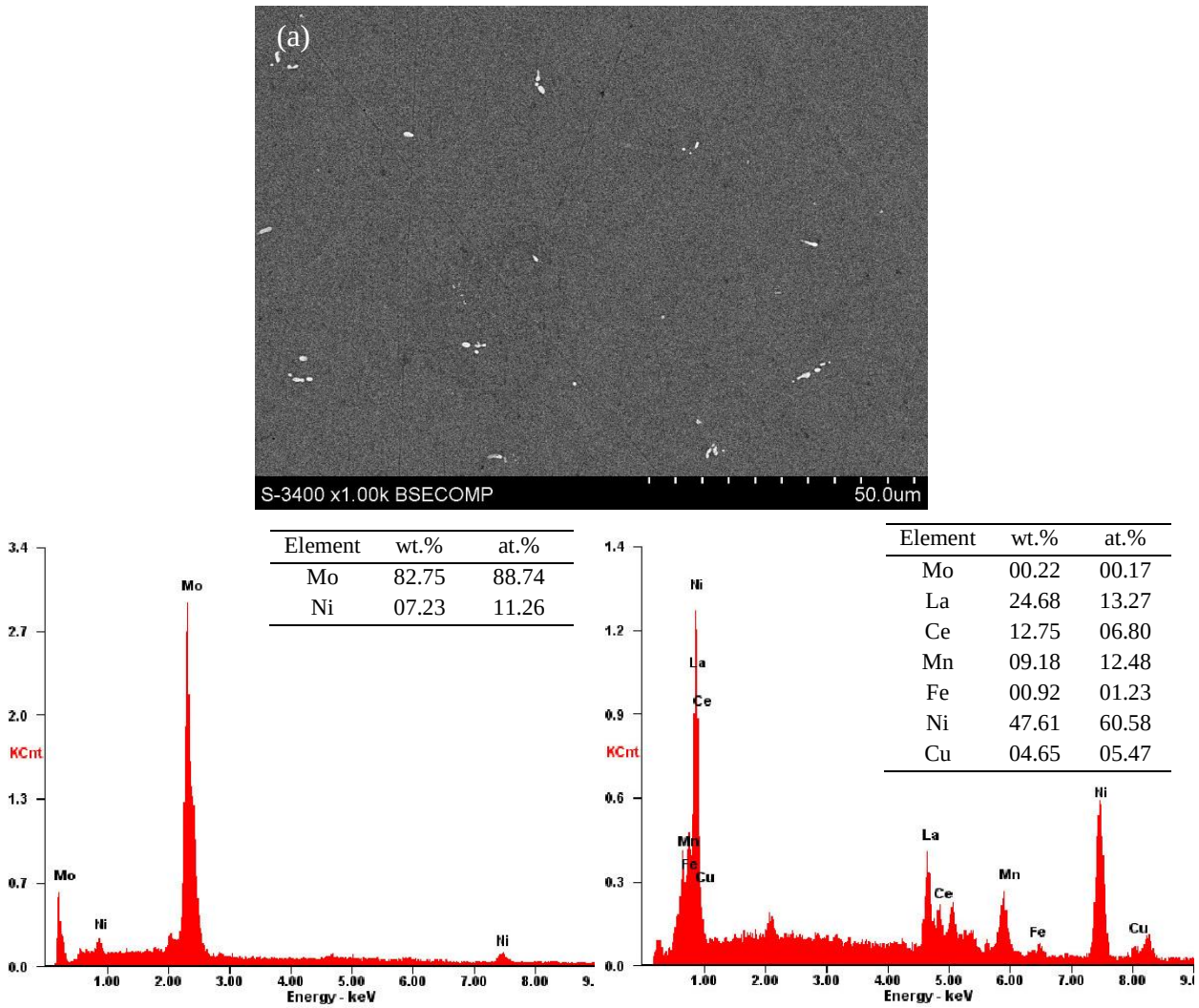

Figure 2. BSE and EDS results of $La_{0.7}Ce_{0.3}Ni_{4.2}Mn_{0.75}Cu_{0.3}(Mo_{0.54}Fe_{0.46})_{0.15}$ alloy (a) BSE (b) EDS of white spots (c) EDS of black grey area

Table 1. Lattice parameters of alloys of $La_{0.7}Ce_{0.3}Ni_{4.2}Mn_{0.9-x}Cu_{0.3}(Mo_{0.46}Fe_{0.54})_x$ alloys

x	*a* (Å)	*c* (Å)	*c/a*	*V* (Å^3)
0	5.0464	4.0835	0.8102	90.06
0.05	5.0344	4.0832	0.8111	89.62
0.10	5.0349	4.0804	0.8104	89.58
0.15	5.0307	4.0716	0.8094	89.24
0.20	5.0271	4.0703	0.8093	89.08

3.2 Maximum discharge capacity and cycling stability

The electrochemical properties of $La_{0.7}Ce_{0.3}Ni_{4.2}Mn_{0.9-x}Cu_{0.3}(Mo_{0.46}Fe_{0.54})_x$ (x= 0-0.20) alloy electrodes are summarized in Table 2. It can be seen that all electrodes can reach the maximum discharge capacity within four charge/discharge cycles, which indicated that the substitution of Mn by $Mo_{0.46}Fe_{0.54}$ alloy plays a little role on the activation performance of alloy electrodes. The maximum discharge capacity (C_{max}) of alloy electrodes monotonically decreases from 332.5 mAh g^{-1} (x = 0) to 310.2 mAh g^{-1} (x = 0.20) with the increment of x value. Similarly, as shown the PCT curves of $La_{0.7}Ce_{0.3}Ni_{4.2}Mn_{0.9-x}Cu_{0.3}(Mo_{0.46}Fe_{0.54})_x$($x$= 0-0.20) alloys in Fig. 3, which can be seen that the hydrogen storage capacity and the plateau pressure gradually decrease with increasing the content of $Mo_{0.46}Fe_{0.54}$ alloy. In general, maximum discharge capacity is related to the crystalline structure and the electrochemical kinetics of the electrode. In this work, the lattice contraction of the alloys and the plateau pressure gradually decrease after the substitution of $Mo_{0.46}Fe_{0.54}$ alloy for Mn, which are detrimental to the maximum discharge capacity of the alloy electrodes. Since the smaller the lattice, the more difficult the diffusion of hydrogen atom [26]. And the decrease of plateau pressure will increase the stability of the hydrides. Worse still is that the increase in Iron content can make the surface oxide film thicker, which not merely degrades the number of activity sites on the alloy surface but also reduces the diffusion rate of hydrogen from the inner to the outer surface or vice versa.

Table 2. Electrochemical properties of $La_{0.7}Ce_{0.3}Ni_{4.2}Mn_{0.9-x}Cu_{0.3}(Mo_{0.54}Fe_{0.46})_x$ alloy electrodes

x	C_{max} (mAh g^{-1})	N_a	HRD_{1200} (%)	S_{100} (%)
0	332.5	4	61.6	79.3
0.05	323.2	4	68.4	73.7
0.10	315.7	4	73.6	69.0
0.15	312.5	4	70.3	67.3
0.20	310.2	4	65.4	62.6

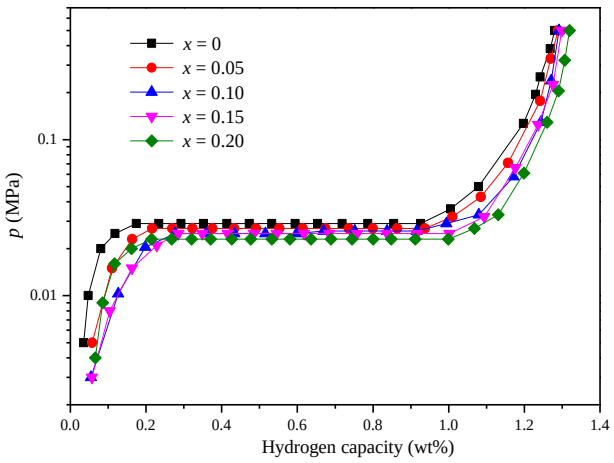

Figure 3. PCT of $La_{0.7}Ce_{0.3}Ni_{4.2}Mn_{0.9-x}Cu_{0.3}(Mo_{0.54}Fe_{0.46})_x$ alloy electrodes at 303 K

The cycle life is an essential performance index of Ni/MH battery, which directly related to the rise and fall of Ni/MH battery development. The capacity retaining rates (S_n) of the alloys at n^{th} charge/discharge cycles can be calculated by the following formula *E*q (1):

$$S_n = C_n/C_{max} \times 100\% \qquad Eq. (1)$$

where C_n is the discharge capacity after n^{th} charge/discharge cycles at the cycle, C_{max} is the maximum dischargecapacity. Fig. 4 shows the electrochemical cyclic stability curves of $La_{0.7}Ce_{0.3}Ni_{4.2}Mn_{0.9-x}Cu_{0.3}(Mo_{0.46}Fe_{0.54})_x$($x$= 0-0.20) alloy electrodes at a discharge current density of 60 mA g^{-1}. It can be seen that the cycling stability of $La_{0.7}Ce_{0.3}Ni_{4.2}Mn_{0.9-x}Cu_{0.3}(Mo_{0.46}Fe_{0.54})_x$($x$= 0-0.20) alloy electrodes present a monotonically deceasing trend with increasing the content of $Mo_{0.46}Fe_{0.54}$ alloy. Table 2 summarizes the value at 100^{th} charge/discharge cycles (S_{100}) of the alloy electrodes. Obviously, S_{100} value monotonically decreases from 79.3% (x = 0) to 62.6% (x = 0.20). As is known to all, the fundamental reasons for the capacity decay of the AB_5-type alloy electrodes are the pulverization and the oxidation of the alloys during charging/discharging cycles [27]. Therefore, the decline of the cycling stability of $La_{0.7}Ce_{0.3}Ni_{4.2}Mn_{0.9-x}Cu_{0.3}(Mo_{0.46}Fe_{0.54})_x$($x$= 0-0.20) alloy electrodes with the substitution of $Mo_{0.46}Fe_{0.54}$ alloy for Mn can be attributed to the following two dominant factors. One is that, as mentioned above, the decrease in *c*/*a* ratio of the main-phase can go against hydrogen atoms from going in and out of the crystal, which can strengthen the lattice stress during charging/discharging cycles and then accelerate the pulverization speed of the alloy electrodes. What's worse, the pulverized alloy creates a fresh surface and then can be oxidized when it comes into contact with KOH electrolyte, which can result in a poor connection among the particles and reduce the electrical conductivity.

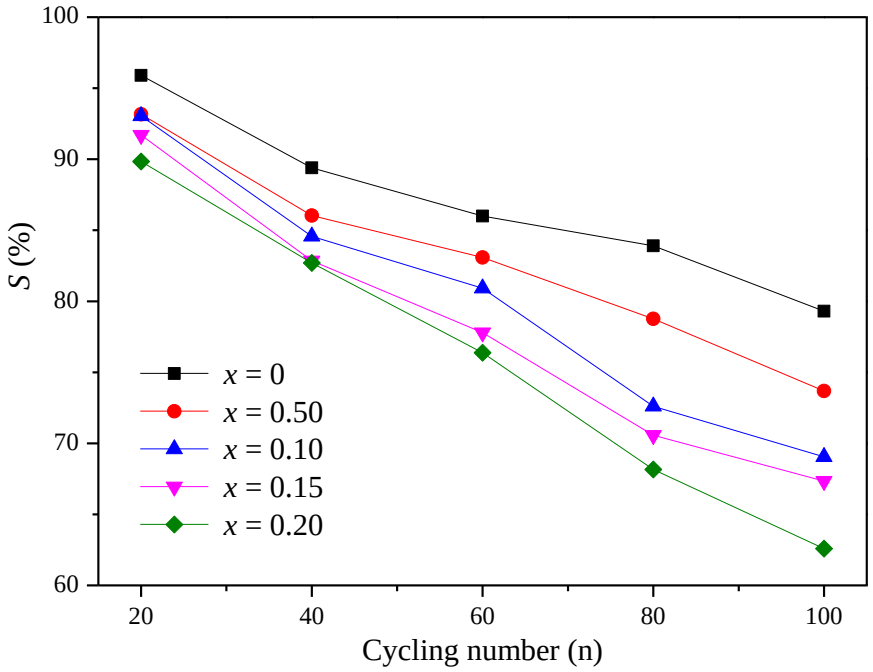

Figure 4. Cycling stability of $La_{0.7}Ce_{0.3}Ni_{4.2}Mn_{0.9-x}Cu_{0.3}(Mo_{0.54}Fe_{0.46})_x$ alloy electrodes at 298 K with the charging/discharging current density of 60 mA g^{-1}

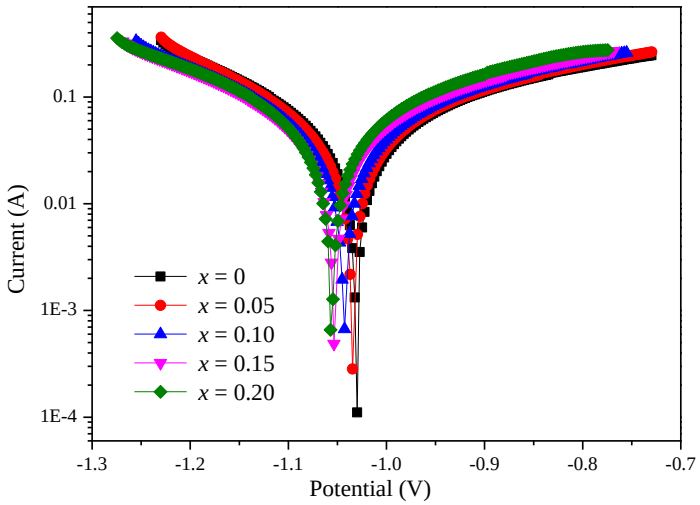

Figure 5. Tafel curves of $La_{0.7}Ce_{0.3}Ni_{4.2}Mn_{0.9-x}Cu_{0.3}(Mo_{0.54}Fe_{0.46})_x$ alloy electrodes at 298 K

The other one is that manganese element is an indispensable element in conventional mischmetal based AB_5-type alloy for maintaining cycle stability [5,7]. Worst of all, as mentioned above, the oxide film formed by Iron can cause the loss of active material and prevents the hydrogen diffusion. Therefore, the increase in iron content is adverse for the cycling stability of the alloy electrodes. In order to further investigate the influence of the substitution of $Mo_{0.46}Fe_{0.54}$ alloy for Mn on the cycle stability of $La_{0.7}Ce_{0.3}Ni_{4.2}Mn_{0.9-x}Cu_{0.3}(Mo_{0.46}Fe_{0.54})_x$($x$= 0-0.20) alloy electrodes, the corrosion behaviors were measured by the technique of potentiodynamic polarization which can be expressed as Tafel curve. Fig. 5 presents the Tafel curves of $La_{0.7}Ce_{0.3}Ni_{4.2}Mn_{0.9-x}Cu_{0.3}(Mo_{0.46}Fe_{0.54})_x$($x$= 0-0.20) alloy electrodes. Clearly, the corrosion potential of the alloy electrodes becomes more negative and the corrosion current increases with increasing x value, which indicates that $La_{0.7}Ce_{0.3}Ni_{4.2}Mn_{0.9}Cu_{0.3}$ alloy electrode has a better anti-corrosion ability than other alloy electrodes containing $Mo_{0.46}Fe_{0.54}$ alloy. Therefore, based on the above reason, it is believed that the decrease in corrosion resistance of alloy electrode is prominent for the degradation of cycling stability in present work.

3.3 High-rate dischargeability and electrochemical kinetic characteristics

The high-rate dischargeability (HRD) behavior is a crucial parameter for practical application of alloys as negative electrode materials of high-power Ni/MH batteries. Fig. 6 shows HRD curves of $La_{0.7}Ce_{0.3}Ni_{4.2}Mn_{0.9-x}Cu_{0.3}(Mo_{0.46}Fe_{0.54})_x$($x$= 0-0.20) alloy electrodes at various current densities and Table 2 lists the values of HRD_{1200}. It can be found that HRD of the alloy electrodes show a variation of the pyramid with increase the content $Mo_{0.46}Fe_{0.54}$ alloy and HRD_{1200} obtain the peak value when x = 0.1 (73.6 %).

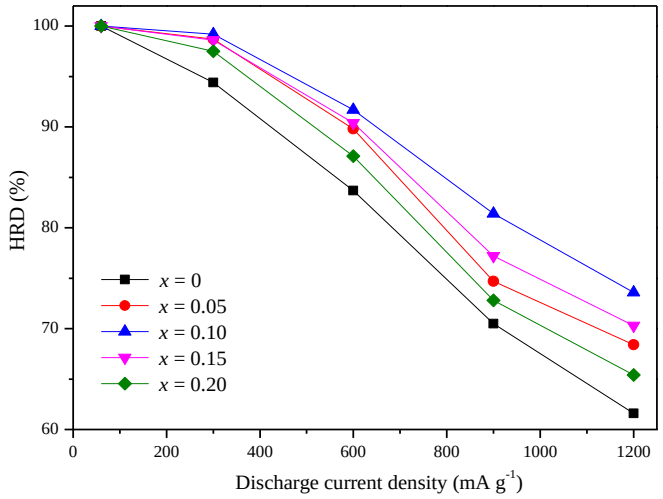

Figure 6. HRD at different discharging current density of $La_{0.7}Ce_{0.3}Ni_{4.2}Mn_{0.9-x}Cu_{0.3}(Mo_{0.54}Fe_{0.46})_x$ alloy electrodes at 298 K

As is known to all, the high-rate dischargeability of Ni/MH battery is mainly dominated by electrochemical kinetics of the alloy electrodes, including the charge-transfer reaction of hydrogen at the alloy/electrolyte interface and the hydrogen diffusion rate from the interior of the bulk to the surface of the alloy particles [28-30]. The two key factors can be evaluated by electrochemical impedance, exchange current density (I_0) and hydrogen diffusion coefficient (D) [31].

Electrochemical impedance spectroscopy can qualitatively reflect the ease and difficulty of charge-transfer on the surface of the alloy electrode [32]. Fig. 7 displays that EIS of $La_{0.7}Ce_{0.3}Ni_{4.2}Mn_{0.9-x}Cu_{0.3}(Mo_{0.46}Fe_{0.54})_x$($x$= 0-0.20) alloy electrodes at 50% depth of discharge and 298 K. Obviously, each EIS spectrum contains two semicircles and a straight line corresponding to two different frequency regions. As elucidated by Kuriyama et al. [33], the semicircle in the high frequency region corresponds to the contact resistance between the alloy powder and the conductive material, while the semicircle in the low frequency region equates to the charge-transfer resistance on the alloy surface. Moreover, the larger the radius of the semicircle in the low frequency region is, the larger the charge-transfer resistance of the alloy electrode will be. Here, EIS was employed to study the R_{ct} value which is summarized in Table 3, and ZSimpWin 3.21 software was used to analyze the experimental data. As shown in Fig. 5, compared to all the alloy electrodes, the radii of the semicircle of each alloy electrodes in the low frequency region are close, which indicated the charge-transfer resistance of $La_{0.7}Ce_{0.3}Ni_{4.2}Mn_{0.9-x}Cu_{0.3}(Mo_{0.46}Fe_{0.54})_x$($x$= 0-0.20) alloy electrodes has been less affected by the substitution of Mn with $Mo_{0.46}Fe_{0.54}$ alloy. Corresponding I_0 value is calculated [34] and also listed in Table 3. It can be found that the value of I_0 almost have no significant change, just like the value of R_{ct}. It was reported that, to a certain extent, manganese element can enhance the charge-transfer process on the alloy surface as well as molybdenum element [17,35]. Therefore, it is quite reasonable that the value of R_{ct} and I_0 are changed little due to the decrease in Mn and the increase in Mo with the increase of MoFe content.

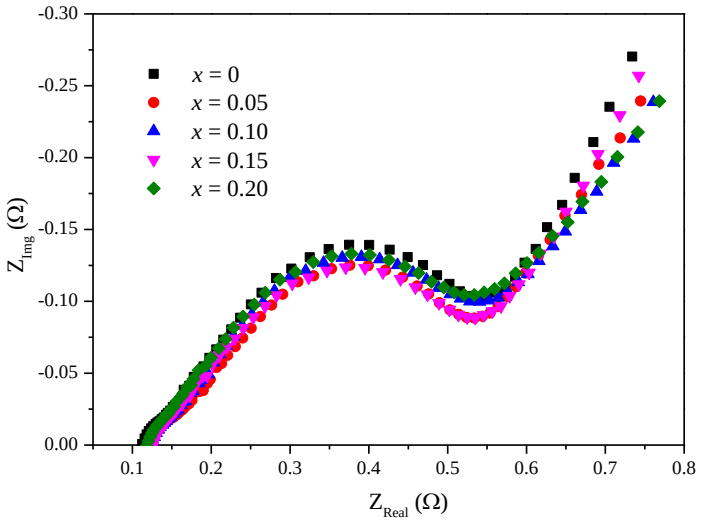

Figure 7. EIS of $La_{0.7}Ce_{0.3}Ni_{4.2}Mn_{0.9-x}Cu_{0.3}(Mo_{0.54}Fe_{0.46})_x$ alloy electrodes at 298 K in the frequency range of 100 kHz to 10 mHz

Table 3. Electrochemical kinetic characteristics of $La_{0.7}Ce_{0.3}Ni_{4.2}Mn_{0.9-x}Cu_{0.3}(Mo_{0.54}Fe_{0.46})_x$ alloy electrodes

x	R_{ct} (mΩ)	I_0 (mA g^{-1})	D (× 10^{-10} cm^2 s^{-1})
0	94.4	272.0	4.20
0.05	91.1	281.8	4.99
0.10	92.7	277.0	5.34
0.15	90.7	283.1	5.26
0.20	93.6	274.3	4.40

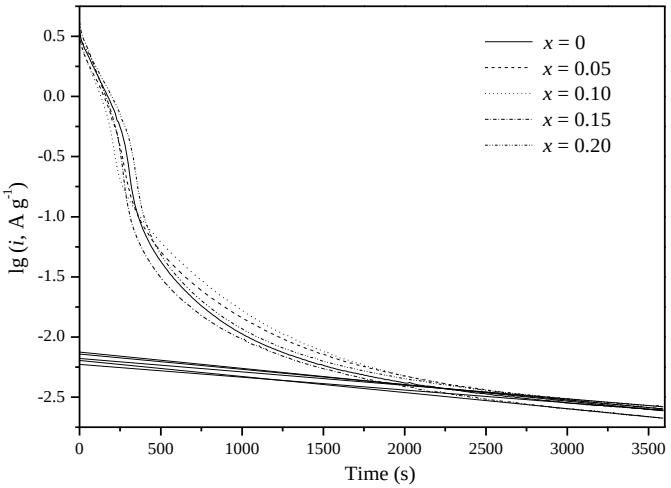

Figure 8. Semilogarithmic curves of anodic current vs. time of response of $La_{0.7}Ce_{0.3}Ni_{4.2}Mn_{0.9-x}Cu_{0.3}(Mo_{0.54}Fe_{0.46})_x$ alloy electrodes at 298 K

The hydrogen diffusion coefficient of $La_{0.7}Ce_{0.3}Ni_{4.2}Mn_{0.9-x}Cu_{0.3}(Mo_{0.46}Fe_{0.54})_x$($x$= 0-0.20) alloy electrodes can be calculated from the slope of the linear region according to the semi-logarithmic plots of the anodic current vs. the time response, which was measured by the means of the potential-step discharge technique and has been shown in Fig.8. The typical calculation method for the value of D has reported in our previous article [36]. Table 3 lists D value of $La_{0.7}Ce_{0.3}Ni_{4.2}Mn_{0.9-x}Cu_{0.3}(Mo_{0.46}Fe_{0.54})_x$($x$= 0-0.20) alloy electrodes. It can be seen that D first increases from 4.20×10^{-10} (x = 0) to 5.34×10^{-10} cm^2 s^{-1} (x = 0.10), while further increasing the value of x jeopardizes D.

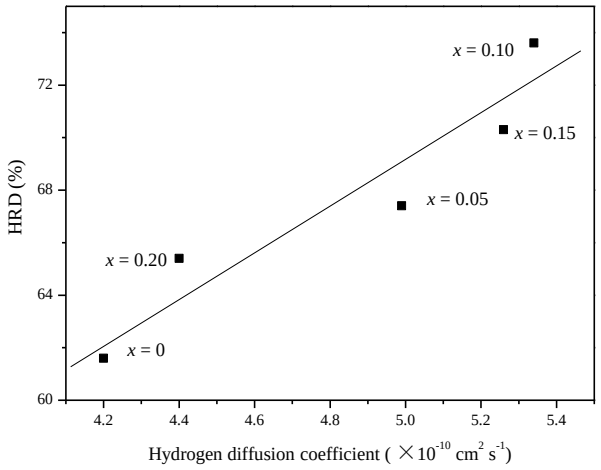

Figure 9. HRD at the discharge current density of 1200 mA g^{-1} as a function of hydrogen diffusion coefficient for $La_{0.7}Ce_{0.3}Ni_{4.2}Mn_{0.9-x}Cu_{0.3}(Mo_{0.54}Fe_{0.46})_x$ alloy electrodes

As Iwakura et al. [29] reported that, if the electrochemical reaction on the surface is the rate-determining factor, a linear dependence of the high-rate dischargeability on the exchange current density should be observed. In contrast, if the diffusion of hydrogen in the bulk is the rate-determining factor, the high-rate dischargeability should be constant, irrespective of exchange density. Fig.9 shows that the HRD at 1200 mA g^{-1} as a function of hydrogen diffusion coefficient for $La_{0.7}Ce_{0.3}Ni_{4.2}Mn_{0.9-x}Cu_{0.3}(Mo_{0.46}Fe_{0.54})_x$($x$= 0-0.20) alloy electrodes. Clearly, HRD_{1200} value of alloy electrodes shows a linear dependence on the value of D, which demonstrated that hydrogen atoms diffusion process in the bulk of alloy plays a more important role in the electrochemical kinetics of the alloys than charge-transfer process at the electrode surface.

4. CONCLUSIONS

The microstructures and electrochemical characteristics of $La_{0.7}Ce_{0.3}Ni_{4.2}Mn_{0.9-x}Cu_{0.3}(Mo_{0.46}Fe_{0.54})_x$($x$ = 0-0.20) hydrogen storage alloys are systematically investigated. The following conclusions can be drawn:

1. Analysis of X-ray diffraction profiles and backscattered electron results shows that the pristine alloy is single $LaNi_5$ phase with a hexagonal $CaCu_5$-type structure, while the alloys containing

$Mo_{0.46}Fe_{0.54}$ consist of $LaNi_5$ matrix phase and a trace of Mo segregate phase. The lattice parameters *a*, *c*, *c*/*a* and *V* of $LaNi_5$ phase decrease after the addition of $Mo_{0.46}Fe_{0.54}$ alloy.

2. The substitution of Mn by $Mo_{0.46}Fe_{0.54}$ alloy plays a little role on the activation performance and all electrodes can reach the maximum discharge capacity within 4 charge/discharge cycles. The maximum discharge capacity of alloy electrodes monotonically decreases from 332.5 (x=0) to 310.2 (x=0.20) mAh g^{-1}.

3. The high-rate dischargeability the alloy electrodes at the discharge current density of 1200 mA g^{-1} first increases from 61.6% (x = 0) to 73.6% (x = 0.10), while further increasing the value of x jeopardizes HRD_{1200}. This is consistent with the variation tendency of hydrogen diffusion coefficient, which indicated that the electrochemical kinetic property is dominated by hydrogen atoms diffusion process in the bulk of alloy.

4. The cycling capacity retention rate at the 100^{th} charge/discharge cycle is decrease monotonously from 79.3 % (x = 0) to 62.6 % (x = 0.20) with increasing the content of $Mo_{0.46}Fe_{0.54}$ alloy, which should be ascribed to the deterioration of corrosion resistance of alloy electrode in the charging/discharging cycle.

ACKNOWLEDGEMENTS
This research is financially supported by the National Natural Science Foundation of China (51671080, 51471065 and U1304522), Plan for Scientific Innovation Talent of Henan Province (144100510009) and Program for Innovative Research Team (in Science and Technology) in the University of Henan Province (16IRTSTHN005).

References

1. T. Erika, C. Sebastian, Z. Fernando, D. Verónica, *Int. J. Hydrogen Energy* 41 (2016) 19684.
2. H. Gan, Y. Yang, H. Shao, *Electrochim. Acta*, 174 (2015) 164.
3. J. Monnier, H. Chen, S. Joiret, J. Bourgon, M. Latroche, *J. Power Sources* 266 (2014) 162.
4. K. Komori, O. Yamamoto, Y. Toyoguchi, K. Suzuki, S. Yamaguchi, A. Tanaka, M. Ikoma, US5512385, 1996.
5. K. Young, D.F. Wong, L. Wang, J. Nei, T. Ouchi, S. Yasuoka, *J. Power Sources* 277 (2015) 426.
6. K. Young, J. Koch, S. Yasuoka, H. Shen, L.A. Bendersky, *J. Power Sources* 277 (2015) 433.
7. T. Sakai, K. Oguro, H. Miyamura, N. Kuriyama, A. Kato, *J. Less Comm. Met*. 161 (1990) 193.
8. J. Kleperis, G. Wojcik, A. Czerwinski, J. Skowronski, M. Kopczyk, M. Beltowska-Brzezinska, *J. Solid State Electrochem.* 5 (2001) 229.
9. J.K. Chang, D.S. Shong, W.T. Tsai, *J. Power Sources* 103 (2002) 280.
10. M. Jing, L. Fang, X. Liu, L. Jiang, Z. Li, S. Wang, *J. Rare Earths* 28(2010) 781.
11. Y. Yan, Y. Chen, C. Wu, M. Tao, H. Liang, *J. Power Sources* 164 (2007) 799.
12. X.B. Zhang, D.Z. Sun, W.Y. Yin, Y.J. Chai, M.S. Zhao, *Electrochim. Acta* 50 (2005) 3407.
13. X.B. Zhang, D.Z. Sun, W.Y. Yin, Y.J. Chai, M.S. Zhao, *J. Power Sources* 154 (2006) 290-297.
14. X.B. Zhang, D.Z. Sun, W.Y. Yin, Y.J. Chai, M.S. Zhao, *J. Inorg. Chem*. 20 (2005) 2235.
15. Y.P. Fan, B.Z. Liu, B.Q. Zhang, L.Q. Ji, Y.G. Wang, Z. Zhang, *Mater. Chem. Phys*. 138 (2013) 803.
16. B.Z. Liu, X.Y. Peng, Y.P. Fan, L.Q. Ji, B.Q. Zhang, Z. Zhang, *Int. J. Electrochem. Sci*. 7 (2012) 11966.

17. V. Díaz, E. Teliz, F. Ruiz, P. S. Martínez, R. Faccio, F. Zinola, *Int. J. Hydrogen Energy* 38 (2013) 12811.
18. H. Ye, H. Zhang, *Adv. Eng. Mater*. 3 (2001) 481.
19. H. Ye, H. Zhang, *Journal of the graduate school of the Chinese academy of sciences*. 2003, 20(3) 381-387.
20. M.T. Yeh, V.M. Beibutian, S.E. Hsu, *J. Alloys Compd*. 293-295 (1999) 721.
21. S.E. Hsu, V.M. Beibutian, M.T. Yeh, *J. Alloys Compd*. 330-332 (2002) 882.
22. S. Basak, K. Shashikala, P. Sengupta, S.K. Kulshreshtha, *Int. J. Hydrogen Energy* 32 (2007) 4973.
23. X.B. Yu, Z.X. Yang, S.L. Feng, Z. Wu, N.X. Xu, *Int. J. Hydrogen Energy* 31 (2006) 1176.
24. X.D. Wei, S.S. Liu, H. Dong, P. Zhang, Y.N. Liu, J.W. Zhu, G. Yu, *Electrochim. Acta*. 52 (2007) 2423.
25. K. Young, T. Ouchi, B. Reichman, J. Koch, M.A. Fetcenko, *J. Alloys Compd*. 509(2011) 3995.
26. X.C. Hu, H.Z. Yan, B.Q. Li, J. Li, L. Wang, W. Xiong, *J. Rare Earths* 32 (2014) 532.
27. D. Chartouni, F. Meli, A. Züttel, K. Gross, L. Schlapbach, *J. Alloys Compd*. 241 (1996) 160.
28. Y. Li, S. Han, J. Li, X. Zhu, L. Hu, *J. Alloys Compd*. 458 (2008) 357.
29. C. Iwakura, T. Oura, H. Inoue, M. Matsuoka, *Electrochimica Acta*. 41 (1996) 117.
30. Y. Sakamoto, K. Kuruma, Y. Naritomi, Berichte der Bunsengesellschaft für physikalische Chemie. 96 (1992) 1813.
31. F. Zhang, Y. Luo, J. Chen, R. Yan, J. Chen, *J. Alloys Compd*. 430 (2007) 302.
32. P. Li, Z. Hou, T. Yang, H. Shang, X. Qu, Y. Zhang, *J. Rare Earths*. 30 (2012) 696.
33. N. Kuriyama, T. Sakai, H. Miyamura, I. Uehara, H. Ishikawa, T. Iwasaki, *J. Alloys Compd*. 202 (1993) 183.
34. G. Zheng, B. N. Popov, R. E. White, *J. Electrochem. Soc*. 142 (8) 2695.
35. C. Zhong, D. Chao, Y. Chen, W. Wang, D. Zhu, C. Wu, *Electrochim. Acta*. 58 (2011) 668.
36. X. Peng, B. Liu, Y. Fan, X. Zhu, Q. Peng, Z. Zhang, *J. Power Sources* 240 (2013) 178.